

## High density Schottky Barrier IRCCD sensors for SWIR applications at intermediate temperature

H. Elabd, T. S. Villani  
RCA Laboratories, Princeton, NJ 08540  
J. R. Tower  
RCA Advanced Technology Laboratories, Camden, NJ 08102

### Abstract

Monolithic 32 x 64 and 64 x 128 palladium silicide (Pd<sub>2</sub>Si) interline transfer IRCCDs sensitive in the 1-3.5 μm spectral band have been developed. This silicon imager exhibits a low response nonuniformity of typically 0.2-1.6% rms, and has been operated in the temperature range between 40-140K.

Spectral response measurements of test Pd<sub>2</sub>Si p-type Si devices yield quantum efficiencies of 7.9% at 1.25 μm, 5.6% at 1.65 μm and 2.2% at 2.22 μm. Improvement in quantum efficiency is expected by optimizing the different structural parameters of the Pd<sub>2</sub>Si detectors. The spectral response of the Pd<sub>2</sub>Si detectors fit a modified Fowler emission model. The measured photo-electric barrier height for the Pd<sub>2</sub>Si detector is ~0.34 eV and the measured quantum efficiency coefficient, C<sub>J</sub>, is 19%/eV.

The dark current level of Pd<sub>2</sub>Si Schottky barrier focal plane arrays (FPAs) is sufficiently low to enable operation at intermediate temperatures at TV frame rates. Typical dark current level measured at 120K on the FPA is 2 nA/cm<sup>2</sup>.

The Pd<sub>2</sub>Si Schottky barrier imaging technology has been developed for satellite sensing of earth resources. The operating temperature of the Pd<sub>2</sub>Si FPA is compatible with passive cooler performance. In addition, high density Pd<sub>2</sub>Si Schottky barrier FPAs are manufactured with high yield and therefore represent an economical approach to short wavelength IR imaging.

A Pd<sub>2</sub>Si Schottky barrier image sensor for push-broom multispectral imaging in the 1.25, 1.65, and 2.22 μm bands is being studied. The sensor will have two line arrays (dual band capability) of 512 detectors each, with 30 μm center-to-center detector spacing. The device will be suitable for chip-to-chip abutment, thus providing the capability to produce large, multiple chip focal planes with contiguous, in-line sensors.

### Introduction

The ambitious goals charted for the next generation of space-borne sensors challenge the state-of-the-art in solid state imaging technology. Next generation satellite surveillance and earth resources sensors will call for visible and infrared focal planes with thousands of detector elements, attendant high fill-factors, and low blemish densities. The requirements are further compounded for infrared focal planes by the desire to operate these large arrays with passive cooling at intermediate temperatures of 120-140K.

The Schottky barrier infrared technology is now at a level of demonstrated performance and maturity that makes it an attractive choice for next generation space-borne sensors. This technology is suitable for Earth sensing applications where moderate quantum efficiency and intermediate operating temperatures are required. Palladium silicide (Pd<sub>2</sub>Si) infrared charge coupled device, IR-CCDs, can operate between 40 and 140K and are sensitive in the short-wave infrared band (1-3.5 μm), whereas platinum silicide (PtSi) IRCCDs, require cooling below 90K but are sensitive in both SWIR and thermal bands (1-5.5 μm). (A paper on PtSi IR-CCDs is presented in the IR Sensor Technology Session of this conference).

The main advantage of this infrared sensor technology is that it is fabricated using standard integrated circuit (IC) processing techniques and commercial IC grade silicon. It is therefore possible to construct high yield Schottky barrier area and line arrays with high density designs and large numbers of blemish-free elements (>8000). A second principal advantage is that Schottky detectors provide inherently high uniformity. Typical photoresponse non-uniformity is on the order of 0.5% RMS for Pd<sub>2</sub>Si detectors. This high uniformity reduces the complexity of electronic compensation, and indeed obviates the need for compensation in many imaging applications. The sensor also exhibits high dynamic range, inherent blooming control, and high linearity at low, as well as, high illumination levels.

The Pd<sub>2</sub>Si technology has been evaluated for NASA Multispectral Linear Array sensor applications.\* This IR-CCD technology is well matched to the operational requirements of the MLA instrument. [1,2,3]

### Schottky barrier sensor technology

The Schottky barrier detector is a photon detector, which utilizes the internal photoemission of "hot" carriers (holes) from metal or metal silicide electrodes into silicon for the detection of optical radiation. Fig. 1 depicts the energy band diagram for the Schottky barrier junction with a simplified one dimensional demonstration of the hole emission process. The back illuminated Schottky barrier detector operates in the spectral window between the band gap of silicon (E<sub>g</sub>) and the barrier height (ψ<sub>ms</sub>). Photons with energies between the bandgap and the barrier height

$$E_g > h\nu > \psi_{ms} \quad (1)$$

will be transmitted through the silicon substrate and will be absorbed in the metal electrode of the junction. The photon energy will increase the potential and kinetic energies of some hole carriers within the metal electrode. Holes traveling in a direction almost normal to the interface with energies larger than the barrier height have a high probability of emission into the silicon substrate.

\*Pd<sub>2</sub>Si testing and MLA sensor studies funded in part by Ball Aerospace Systems Division as part of the BASD "Multispectral Linear Array Instrument Definition Study", NASA GSFC Contract NAS5-26590, March 1982.

To enhance the number of photocarriers injected in the substrate for a certain Schottky barrier height, it is important to thin down the silicide layer to below the attenuation length of the photoresponse. Improvement in the injection efficiency is usually achieved with thin silicide layers typically in the range between 20-100Å. The improvement is the result of reflections of excited carriers by the back surface at the silicide-dielectric interface, minimal reflection of incident radiation at the silicon-silicide interface and enhanced optical absorption within the attenuation length by the multiple pass induced by an aluminum reflector.

The barrier height determines the cut-off wavelength ( $\lambda_c$ ), dark current ( $J_D$ ), maximum operating temperature ( $T_{max}$ ), quantum efficiency ( $Y$ ) and the responsivity ( $R$ ) of the Schottky barrier detector at low temperature according to the following equations:

$$\lambda_c = 1.24/\psi_{ms} \quad \text{microns} \quad (2)$$

$$J_D = A^*T^2e^{-q\psi_{ms}/kT} \quad \text{A/cm}^2 \quad (3)$$

$$T_{max} \sim 425 \psi_{ms} \quad \text{K} \quad (4)$$

(for  $J_{Dmax} = 10^{-7} \text{ A/cm}^2$ )

$$Y = C_1 [h\nu - \psi_{ms}]^2/h\nu \quad \text{electrons/photon} \quad (5)$$

$$R = C_1 [1 - \psi_{ms} \lambda/1.24]^2 \quad \text{A/W} \quad (6)$$

where  $\psi_{ms}$  is the barrier height in eV,  $A^*$  is the Richardson constant,  $T$  is the absolute temperature in degrees Kelvin,  $q$  is the electronic charge,  $k$  is the Boltzmann constant,  $C_1$  is the quantum efficiency coefficient of the modified Fowler emission model,  $h\nu$  is the photon energy and  $\lambda$  in the wavelength in microns.

There is a trade-off between the maximum operating temperature and the cut-off wavelength as shown in equations (2) and (4). The maximum operating temperature is calculated from equations (3) and (4) assuming a dark current density of  $10^{-7} \text{ A/cm}^2$ , estimated from typical thermal imaging dynamic range and dark current shot noise considerations. This trade-off is demonstrated in Table 1 for different silicide electrodes. Fig. 2 is a graphical representation of this trade-off. The locus of the maximum operating temperature for different wavelengths may be approximated by  $\lambda_c T_{max} \sim 527$ .  $\text{Pd}_2\text{Si}$  arrays with a  $3.5 \mu\text{m}$  cut-off wavelength can operate up to 145K, whereas two types of PtSi arrays with  $5.5 \mu\text{m}$  and  $6.0 \mu\text{m}$  cut-off wavelength have maximum operating temperatures of 90K and 85K respectively. NiSi,  $\text{WSi}_2$ , and  $\text{TiSi}_2$  Schottky barrier detectors have cut-off wavelengths around  $2.5 \mu\text{m}$  and maximum operating temperature in the range between 180 and 200K. Extended long-wavelength spectral response can be achieved at temperatures below 77K by using IrSi electrodes or shallow barrier lowering p-type implants.

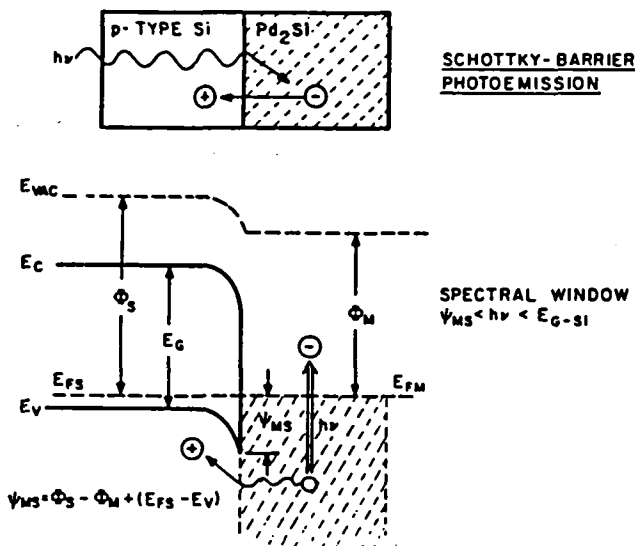


Fig. 1. Energy band diagram.

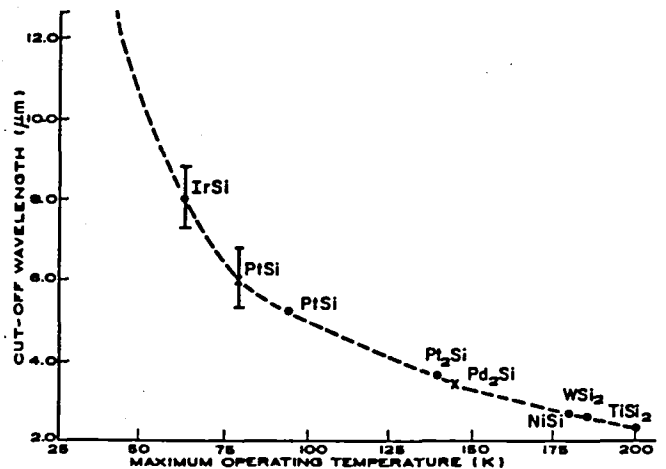


Fig. 2. Maximum operating temperature of various Schottky Barrier technologies

#### Detector and FPA responsivities

The detector responsivity model (equation 6) corresponding to the modified Fowler emission is shown to fit the measured spectral response of PtSi and  $\text{Pd}_2\text{Si}$  Schottky barrier detectors presented on Fig. 3. By comparing the responsivity data, it is evident that, at the present time, the PtSi detectors are more sensitive in the SWIR band than  $\text{Pd}_2\text{Si}$ -detectors by a factor of 3 or higher. A typical value of the  $C_1$  coefficient of the PtSi detectors is 54.2% as compared to a  $C_1$  coefficient of 19.1% for the first generation  $\text{Pd}_2\text{Si}$  detectors. Further optimization of the quantum efficiency of the  $\text{Pd}_2\text{Si}$  detectors is possible. This should be achieved by improving the  $C_1$  coefficient, which is dependent on the stoichiometry, thickness of the silicide layer, and the junction depth. We project the following quantum efficiencies for  $\text{Pd}_2\text{Si}$  detectors in the MLA-SWIR bands: 20.0% at  $1.25 \mu\text{m}$ , 14.0% at  $1.65 \mu\text{m}$  and 5.5% at  $2.2 \mu\text{m}$ .

TABLE 1. SCHOTTKY BARRIER SPECTRAL RESPONSE - OPERATING TEMPERATURE TRADE-OFF

SILICIDE	MEASURED VALUES OF $\phi_{BN}$ (EV)	MEASURED OR CALCULATED VALUES OF		
		$\psi_{MS}$ (EV)	$\lambda_c$ ( $\mu m$ )	MAX. OPERATING TEMP (K) $J_D = 1.0 \times 10^{-7}$ A/CM <sup>2</sup>
IRSi	0.93-0.94	<0.18	>7.0	55-65
PtSi	0.88	0.19-0.20	~6.0	<90
Pt <sub>2</sub> Si	0.78	0.35	3.65	140
Pd <sub>2</sub> Si	0.74	~0.34	~3.6	145
NiSi	0.66	0.46	2.7	180
WSi <sub>2</sub>	0.65	0.47	2.64	185
TiSi <sub>2</sub>	0.60	0.52	2.4	200

The Schottky barrier focal plane (FPA) responsivity,  $R_{FPA}$  in Volts/Watt and Volts/Photon can be calculated from the following equations:

$$R_{FPA} = R \frac{t_{int} \tau_o \eta_{ff} G}{C_{FD}} \quad V/W \quad (7a)$$

$$R \text{ (Volts/Photon)} = R_{FPA} \text{ (V/W)} / h\nu \text{ (Joule)} \quad (7b)$$

where R is the detector responsivity as calculated from equation (6),  $t_{int}$  is the optical integration time,  $\tau_o$  is the transmission of the optics,  $\eta_{ff}$  is the fill factor (the ratio of the detector area to the pixel area), G is the gain of the output amplifier and  $C_{FD}$  is the capacitance of the floating diffusion amplifier. The FPA responsivity is reduced by the duty factor of the detector if the integration time is less than the frame time.

The high responsivity attained with the 32 x 64 PtSi-SB area array is demonstrated in Fig. 4. This interline transfer array has a 25% fill factor and operates at a 60 frames per second rate,  $G = 0.5$  and  $C_{FD} = 0.16$  Pf. For comparison we note here that PtSi SB-FPA responsivity is comparable to that of the InSb-line array with higher fill factor and longer frame time ( $t_{int} = 40$  m sec). The InSb-FPA voltage responsivity at  $\lambda = 2.65 \mu m$  is  $9 \times 10^9$  V/W.[4] Whereas the PtSi-FPA responsivity is  $3 \times 10^9$  V/W at the same wavelength. The PtSi-FPA voltage responsivity in the thermal band is lower and typically in the range between  $1.5 \times 10^9$  and  $1.5 \times 10^8$  V/W. This responsivity is still sufficient to resolve 0.1°C temperature difference in the PtSi-FPA thermal imagery.

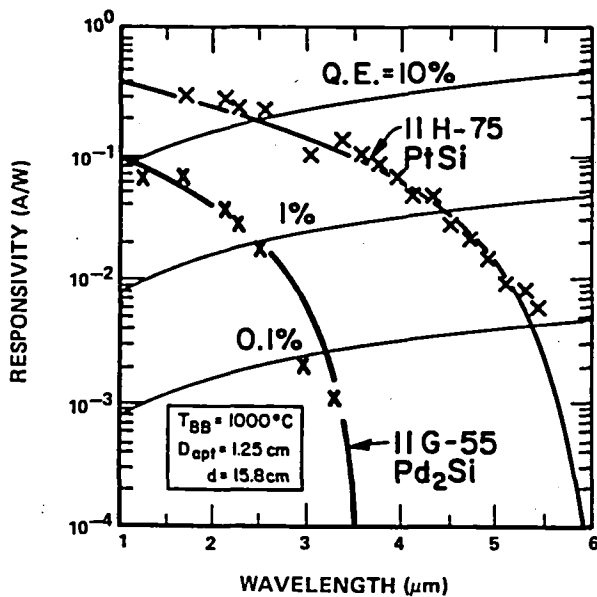


Fig. 3. Measured responsivity of first generation Pd<sub>2</sub>Si and recent PtSi detectors.

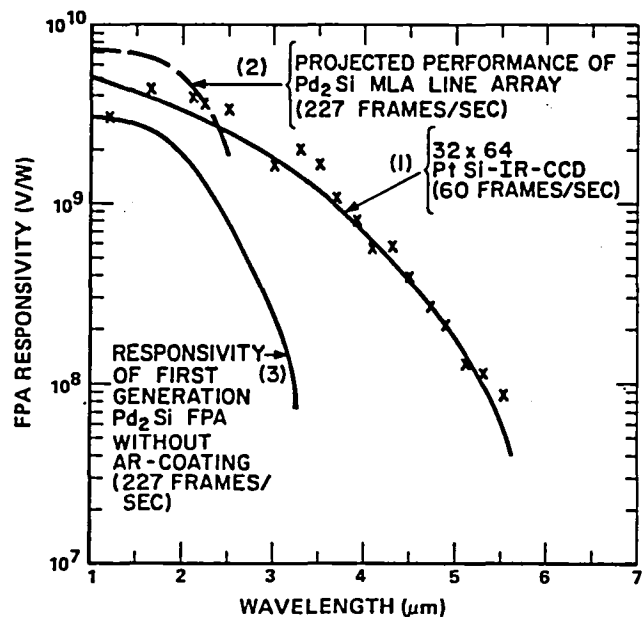


Fig. 4. FPA responsivity for PtSi and Pd<sub>2</sub>Si arrays.

The measured Pd<sub>2</sub>Si detector responsivity was used to calculate the MLA linear array responsivity for 30μ x 30μ detectors at an 80% fill factor, 4.4 msec integration time, G = 0.5 and C<sub>FD</sub> = 0.05 Pf. This Pd<sub>2</sub>Si-FPA responsivity is compared in Fig. 4 to the projected Pd<sub>2</sub>Si-responsivity for an MLA linear array. This design goal is based on the projected quantum efficiency of next generation Pd<sub>2</sub>Si detectors with AR-coating.

Schottky barrier detectors are characterized by a gradual spectral cut-off characteristic. This cut-off characteristic can be evaluated from the derivative of the quantum efficiency (equation 5):

$$\frac{1}{Y} \frac{dY}{d\lambda} = \frac{1}{\lambda} [1 - 2/[1 - \psi_{ms} \lambda/1.24]] \quad (8)$$

From this relationship the relative spectral response uniformity is calculated for Pd<sub>2</sub>Si detectors (ψ<sub>ms</sub> ~ 0.34 eV). The relative response of Pd<sub>2</sub>Si detectors will not deviate from the average response for a 100 nm interval between 1.1 μm and 2.4 μm by more than 10%. This guarantees a relatively flat spectral response. The PtSi detectors with a lower barrier (ψ<sub>ms</sub> ~ 0.21 eV) are capable of higher quantum efficiency and a more gradual cut-off characteristic.

#### SWIR-FPA read-out structure

The construction of the Schottky barrier detector (SBD) readout structure is illustrated on Fig. 5(a). This cross section shows the detector and the BCCD channel isolated by P+ channel stops. The N<sup>-</sup> BCCD implant is used to form N<sup>-</sup> guard rings around the detector. The detected charge signal is coupled from the SBD to the BCCD by an n+ diffusion and a surface channel transfer gate. Fig. 5b illustrates the voltage reset (vidicon) readout mode. During the integration period, t<sub>int</sub> (the time between two successive reset operations) the surface channel barrier is high to isolate the detector from the CCD channel. The detector is reverse biased (V<sub>R</sub> ≥ 8 volt) by the reset pulse on the transfer gate V<sub>T</sub>. The photo-charge is accumulated on the detector node capacitance and transferred to the CCD at the end of the integration time by resetting the SBD to channel potential level (2).

The detected charge, Q<sub>D</sub> is related to the change of the detector voltage, ΔV<sub>D</sub>, by the following equation:

$$Q_D = C_D \Delta V_D \quad (9)$$

where C<sub>D</sub> is the SBD node capacitance.

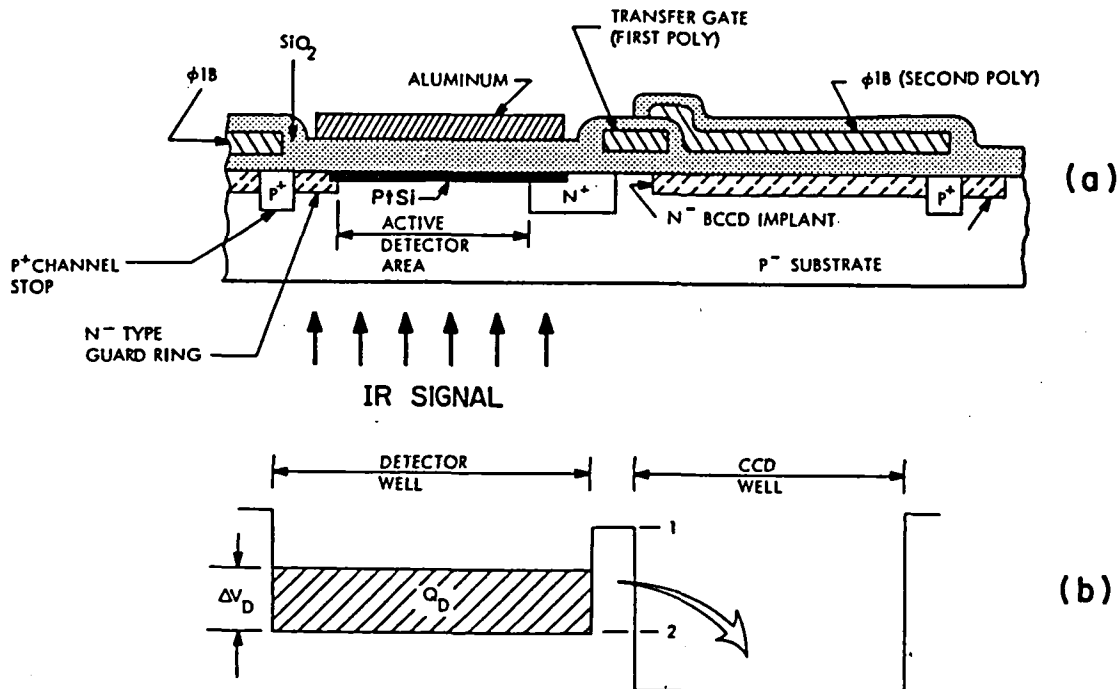


Fig. 5. SBD vidicon readout structure.

The breakdown voltage of the silicon SBD is 35-45 Volt, which is higher than that of junctions formed in narrow bandgap IR-material (HgCdTe). Therefore, the voltage reset readout mode with reset pulse amplitudes higher than 20V can be used in conjunction with SBD arrays. In addition, the quantum efficiency of SB detectors allow their operation with 100% duty cycle for typical thermal imaging and space (MLA) applications. Therefore, the detector integrates photons during the entire frame time and only one reset operation per frame is needed. The once-per-frame detector-to-CCD transfer of charge packets is more immune to CCD gate threshold and trapping nonuniformities than the direct injection readout mode [5]. The direct injection readout mode, also called source modulation or continuous charge skimming, is attractive for detector junctions formed in narrow bandgap IR-material since it requires minimal detector bias which reduces dark current nonuniformities and the reverse breakdown problems. However, for low background SWIR applications the small current densities

flowing from HgCdTe detectors to a CCD in the direct injection mode result in increased sensitivity to CCD input nonlinearity and nonuniformity. Therefore, gate coupling is a preferred readout technique for compound semiconductor SWIR detectors [6] in spite of the inherent fixed pattern noise and nonlinearity associated with that CCD input technique.

The measured optical transfer characteristics for Schottky barrier detectors with vidicon mode readout is illustrated in Fig. 6. This measurement was performed with a 32 x 64 PtSi array (3-5  $\mu\text{m}$  band) at 77K. The net optical densities ( $\tau_0$ ) of the neutral density filters used in the test are indicated below the curve. The change in the output voltage above the value corresponding to the thermal background is linear with irradiance (slope = 1) from the noise equivalent irradiance, until the saturation irradiance of the detector.

### Electrical characteristics

The Pd<sub>2</sub>Si Schottky barrier detector exhibits ideal electrical characteristics below 200K. Typical Pd<sub>2</sub>Si dark current density at 120K is 2 nA/cm<sup>2</sup> (at a transfer voltage of  $\sim 10$  volts). The dark current of the Pd<sub>2</sub>Si detector at 120K is considerably less than that of PtSi at 77K.

The measured dark current-temperature characteristic of PtSi and Pd<sub>2</sub>Si Schottky barrier detectors fit the Richardson thermionic emission model (equation (3)), as shown in Fig. 7. The curves are fitted to equation (3) to evaluate the electrical barrier height (activation energies): 0.20 eV for PtSi and 0.37 eV for Pd<sub>2</sub>Si.

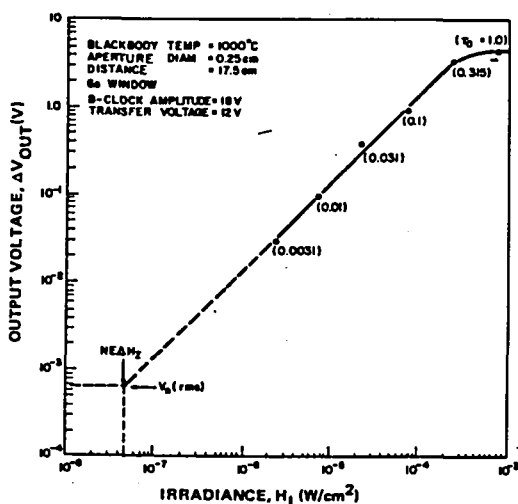


Fig. 6. Photoresponse linearity of Schottky barrier FPAs with vidicon readout mode.

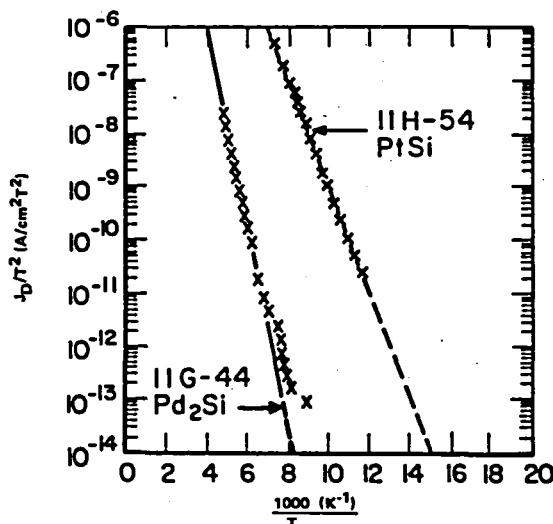


Fig. 7. Measured dark current-temperature characteristics for Pd<sub>2</sub>Si and PtSi detectors.

### Test imagery

The rms non-uniformity,  $g$ , of the output video of the SWIR array may be approximately estimated from this empirical formula:

$$g = \frac{\Delta V_{p-p}}{6 V_{out}} = \frac{\Delta V_{p-p}}{6 m V_m} \quad (10)$$

where  $\Delta V_{p-p}$  is the peak-to-peak nonuniformity in a frame of video displayed on a scope under uniform illumination,  $V_{out}$  is the mean output voltage at the same exposure,  $m$  is the filled fraction of the detector well, and  $V_m$  is the output voltage corresponding to a full detector well. Measurements made on the 32 x 64 Pd<sub>2</sub>Si-FPA at 120K indicate high response uniformity,  $g = 0.2\%$  at  $m = 0.16$ ,  $g = 0.4\%$ - $1.6\%$  at  $m = 0.008$ .

Figs. 8 and 9 demonstrate SWIR-Pd<sub>2</sub>Si imagery obtained without electronic compensation at 130K. These images were produced with a blemish-free 32 x 64 (>2000 detectors) area array (Fig. 9) and an array with one defective diode (Fig. 8). The images were sensed in the dark with a remote SWIR radiation source (1-3  $\mu\text{m}$ ) directed towards the objects. The Pd<sub>2</sub>Si-FPA operating behind variable aperture Si optics ( $f/\# \sim 1.5$ ) was used to detect the radiation reflected from the skin. This skin reflectance at room temperature is above 30% between 1.0  $\mu\text{m}$  and 1.5  $\mu\text{m}$  and drops below 10% for longer wavelengths. In addition a video tape was recorded of outdoor imagery in the SWIR band using daytime reflected sun light. The scene contrast changed depending on the time of the day and intensity of solar radiation. Similar SWIR imagery have been produced by 64 x 128 FPAs.

The charge integration process in the vidicon readout mode is self-limiting and no blooming occurs during optical overload. The difference in the turn-on voltage of the Schottky detector and the parallel n<sup>+</sup>p junction is 0.3-0.5 volt. Therefore the CCD channel will not be flooded with electrons even if the Schottky detector is forward biased during optical overload. In addition, the Pd<sub>2</sub>Si detector with vidicon readout has high dynamic range, 70 dB, and high MTF, 65%, calculated for the proposed MLA sensor array. The high MTF of the Schottky barrier array imagery is the result of the fact that the carrier generation and collection occur in the same thin silicide layer (no carrier diffusion to adjacent detectors occurs as in some visible CCD imagers). The resulting imagery tends to be of higher quality than expected from a 32 x 64 element array.



Fig. 8. Pd<sub>2</sub>Si SWIR imagery of a man smoking a cigar (uncompensated at 130K).



Fig. 9. Pd<sub>2</sub>Si SWIR imagery of a face (uncompensated at 130K).

#### MLA application

The MLA instrument [3] will have several distinct advantages compared to present satellite-borne remote sensing systems [Table 2]. For comparison, the current imaging systems in the Landsat program, the Multispectral Scanners (MSS) and the Thematic Mapper (TM), use mechanical scanner technology to provide image information in the cross-track direction. The MLA however will use the satellite's motion to scan large solid state detector line arrays in a 185Km wide swath on the earth's surface as shown in Fig. 10. This "pushbroom" mode of operation will have the obvious benefits of increased dwell time, potentially higher spatial resolution, and inherent reliability. Furthermore, by simply adjusting the sensor read-out rate (i.e., variable integration time), multi-altitude capability is achieved, which is something inconceivable in mechanical scanned system due to loss of contiguity between stripes of data. Table 2 compares the system capabilities of the MSS, TM, and MLA sensors [7, 8, 9]. It is planned that there will be six spectral bands in the MLA instrument, four bands in the visible (VIS) and near-IR (NIR) and two bands in the SWIR. An additional thermal IR band (TIR) may be added. The desired ground resolution across the 185Km swath is 15 meters in the visible/near-IR bands and 30 meters in the SWIR bands. These specifications call for 12,288 detectors per band in the visible/near-IR and 6,144 detectors in each of the two SWIR bands. Furthermore, it may be desirable that both SWIR bands be placed in close proximity on the same substrate in order to attain maximum band-to-band alignment accuracy. The two SWIR bands will be chosen from the three bands currently under study, 1.25  $\mu$ , 1.65  $\mu$ , and 2.22  $\mu$ .

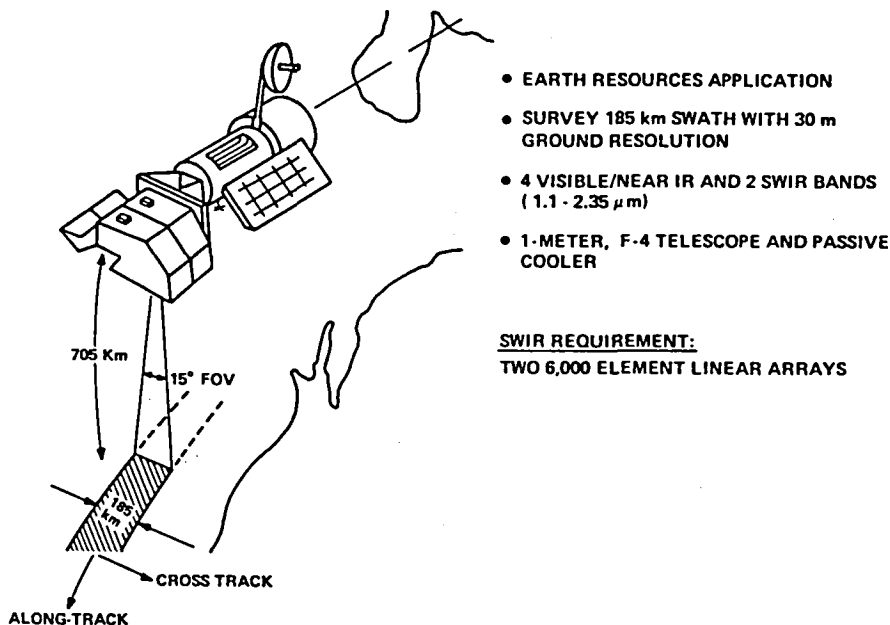


Fig. 10. MLA instrument system concept.

TABLE 2. COMPARISON OF MSS, TM, AND MLA SENSORS

	MSS		TM	MLA
Nominal Altitude	918 km		705 km	705 km (free flyer, current design)
Multialtitude capability	Loss of contiguity of data strips			Yes
Scene Scan	Oscillating mirror, image in forward sweep only		Oscillating mirror image in forward and back sweep	Staring array - Pushbroom
Dwell time at 705 km orbit	> 10 $\mu$ sec		VIS/NIR/SWIR 10 $\mu$ sec TIR 40 $\mu$ sec	4.4 m sec
Spectral bands ( $\mu$ m)	VIS	0.5 - 0.6 0.6 - 0.7 0.7 - 0.8	0.45 - 0.53 0.52 - 0.60 0.63 - 0.69	0.45 - 0.52 0.52 - 0.60 0.63 - 0.69
	NIR	0.8 - 1.1	0.76 - 0.90	0.76 - 0.90
	SWIR		1.55 - 1.75 2.08 - 2.35	1.55 - 1.75 2.08 - 2.35
	TIR		10.4 - 12.5	(10.0 - 12.0)
Detectors per band	6		16 VIS/NIR/SWIR 4 TIR	12,288 VIS/NIR 6,144 SWIR (1,843 TIR)
Ground resolution	80 m		30 m VIS/NIR SWIR 120 m SWIR	15 m VIS/NIR 30 m SWIR (120 m TIR)
Quantization	1.56% 6 bits		0.39% 8 bits	< 0.39% > 8 bits
Sensor pointing modes	Nadir		Nadir	- Nadir - Fore-aft stereo - Cross-track

Pd<sub>2</sub>Si staring FPA cameras may be used as radiometers in different SWIR spectral windows to measure target reflectance. The voltage response,  $V_\lambda$ , of the FPA at wavelength  $\lambda$  for reflected radiation from a resolved target is:

$$V_\lambda = R_{FPA,\lambda} \left[ \frac{W \rho \tau_a A}{4\pi f/\#^2} \right] = p\rho \quad (11)$$

where  $R_{FPA,\lambda}$  is the voltage responsivity of the FPA at wavelength  $\lambda$ ,  $W$  is the scene illumination intensity in  $W/cm^2$ ,  $\rho$  is the target reflectivity,  $\tau_a$  is the atmospheric transmission,  $f/\#$  is the optics focal ratio,  $A$  is the pixel area and  $p$  is the voltage-reflectance proportionality factor.

The output voltage of the camera is proportional to the target reflectivity. Thus, target reflectivity,  $\rho$ , can be estimated by calibrating the FPA output in response to several targets of known reflectance at the identical illumination intensity. In this case, the  $NE\Delta\rho$ , the rms noise equivalent reflectance change from a background reflectance  $p$  at a scene illumination  $W$ , is determined by the IRCCD noise equivalent signal, NES, in rms electrons, at the same exposure

$$NE\Delta\rho = \left[ \frac{4\pi q f/\#^2}{R t_{int} \tau_o \tau_a W A \eta_{ff}} \right] (NES) \quad (12)$$

Clearly  $NE\Delta\rho$  is a function of the atmospheric transmission and scene illumination at the time of the measurement. The noise equivalent signal (NES) is the rms summation of: (1) the signal generated shot noise, (2) KTC noise sources, (3) MOSFET noise, and (4) CCD noise. The NES signal, at or above the working level irradiance (WLI), is dominated by the signal photon generated shot noise and some CCD low temperature transfer loss noise (for long CCD arrays). Equation (12) neglects the radiometric error generated by the temperature uncertainty between the time of calibration and the time of the measurement as well as the quantization errors. Table 3 demonstrates the required radiometric resolution [10], for the SWIR bands. These calculations assume typical working level irradiance in the image plane, and the corresponding scene illumination based on  $f/\# = 3$ ,  $\tau_o \tau_a = 60\%$  and 100% scene reflectance.  $NE\Delta\rho$  values are calculated based on  $t_{int} = 4.4$  msec,  $A = 9 \times 10^{-6} cm^2$ ,  $\eta_{ff} = 0.85$ , NES values of 721, 638 and 414 (electrons) in SWIR bands 1 to 3 respectively, and the Pd<sub>2</sub>Si projected quantum efficiency. Clearly the projected  $NE\Delta\rho$  for the Pd<sub>2</sub>Si arrays is better than the required ( $NE\Delta\rho$ ) radiometric resolution.

Alternatively, the target reflectivity,  $\rho$ , can be evaluated by comparing the output of the FPA corresponding to the target,  $V_T$ , to that due to a reference surface,  $V_r$ , of known reflectivity  $\rho_r$  [11]:

$$\rho = \frac{V_T - V_D}{V_r - V_D} \rho_r \quad (13)$$

where  $V_D$  is the dark level voltage. Equation (13) assumes that both the target and the reference are illuminated by the same irradiance.

TABLE 3. RADIOMETRIC PERFORMANCE OF Pd<sub>2</sub>Si SENSOR

Band	Required NEΔρ	WLI (μW/cm <sup>2</sup> )	Scene Radiance (W:mW/cm <sup>2</sup> .Sr)	Projected (NEΔρ)	Limit Error in Relative Measurement of 10% Reflectance
1.2–1.3 μm (1)	1.0%	9.2	0.55	0.19%	0.1±0.0015
1.55–1.75 μm (2)	1.0%	7.2	0.43	0.22%	0.1±0.002
2.08–2.35 μm (3)	2.4%	3.5	0.21	0.56%	0.1±0.006

The maximum fractional uncertainty in the reflectance measurement described above is given by:

$$\frac{\Delta\rho_{\max}}{\rho} = (S/N)_T^{-1} + (S/N)_R^{-1} + \left(\frac{1}{V_R} + \frac{1}{V_T}\right) (2\bar{Q} + DNES) + TCE \quad (14)$$

where  $(S/N)_T$  and  $(S/N)_R$  are the signal-to-noise ratio of the target and reference measurements,  $\bar{Q}$  the quantization error in the A/D converter, DNES is the noise equivalent signal at no illumination and TCE is the radiometric error due to temperature calibration uncertainty between the reference and the target measurements (calibration uncertainty between the reference and target measurements caused by changes in the level and shot noise of detector dark current). For the Pd<sub>2</sub>Si-FPA operating at 120K with 1°C temperature uncertainty, this TCE error is negligible.

At the photon shot noise limit for short line arrays with negligible detector 1/f noise, neglecting DNES error in comparison to the noise equivalent signal under illumination (NES), the limit uncertainty is given by:

$$\frac{\Delta\rho_{\max}}{\rho} = \sqrt{\frac{qG}{C_{FD}P}} \left[ \frac{1}{\sqrt{\rho}} + \frac{1}{\sqrt{\rho_R}} \right] + \frac{2\bar{Q}}{P} \left[ \frac{1}{\rho} + \frac{1}{\rho_R} \right] + TCE \quad (15)$$

Using equation (15) we calculate the limit fractional uncertainty in a 10% target reflectance measured by comparing to a 100% reflectance, assuming 1 Volt: 4096 quantization. In Table 3 we show these maximum fractional error values calculated for this relative measurement. Increasing the A/D resolution reduces this maximum fractional uncertainty.

MLA sensor design

The sensor envisioned for the MLA application would consist of multiple chips placed end-to-end to produce the desired two linear arrays of 6,144 detectors each. Each chip would consist of two rows of detectors with on-chip CCD multiplexers and associated output amplifiers. The overall module configuration for this monolithic integrated circuit is shown in Fig. 11. A 512 x 2 dual band device is thought to be the optimum choice considering yield, data-rates, and focal plane complexity. This would result in a twelve chip MLA focal plane. There is confidence in proposing this 1024 detector module based upon the demonstrated yield in the technology. Of particular note is that blemish-free 64 x 128 Schottky-barrier area arrays have been fabricated [12].

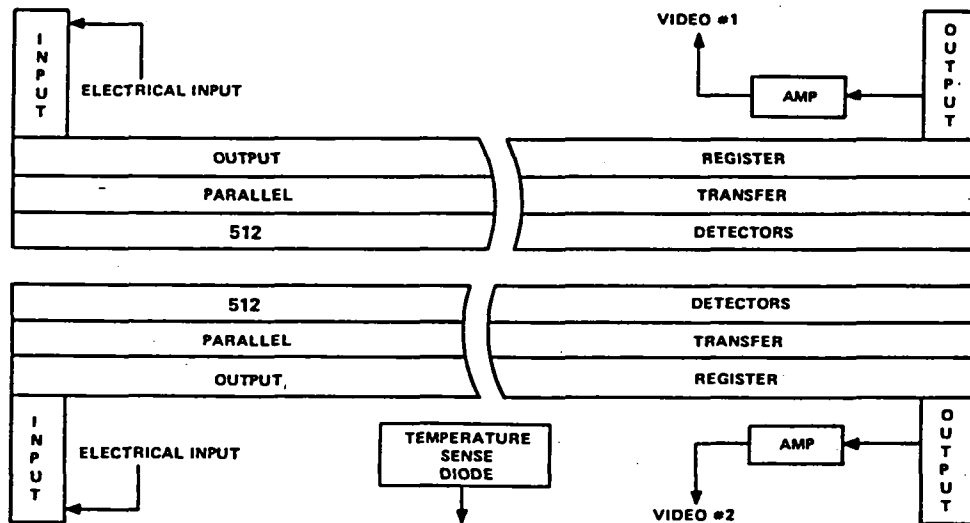


Fig. 11. MLA dual band sensor design.

Mechanical end-to-end butting is the preferred butting technique. It avoids the vignetting and optical/mechanical alignment problems found in optically butted systems, as well as, the tight chip packaging (along-track) and data reformatting required in staggered offset configurations. Experiments indicate that end-to-end butting may be done with less than 40  $\mu$  inactive area across the abutment seam (20  $\mu$  on each chip edge). This would permit a minimal loss of image data at the eleven abutment seams required for a twelve chip focal plane.

The packaging concept for an MLA focal plane may be seen in Fig. 12. The chips are back-side illuminated through a baffled aperture. The cold mount would be attached to the package cover. The package material studied has an excellent match of thermal expansion coefficient to that of the silicon chips. Based on experience with visible CCD imagers [13] operating at room temperature, and calculations of low temperature induced stresses, it appears that this packaging concept would maintain 5  $\mu$  alignment tolerances (chip-to-chip).

The desirable detector pitch (center-to-center spacing) for the MLA instrument is 30  $\mu$ m. This pitch would result in a focal plane with a 7.25" active scanning dimension. This aggressive pitch is coupled with a fill-factor requirement of 85% active area per 30  $\mu$  x 30  $\mu$  detector.

The power dissipation and operating temperature of the dual band sensor are important figures of merit. The dissipation of the 2 x 512 sensor is projected to be 11 mW at the nominal data rate. Thus, the full twelve chip focal plane would dissipate 132 mW, which is well within the passive cooler performance range (typically 1 Watt at 120K operating temperature).

Table 4 summarizes the projected performance for an MLA dual band Pd<sub>2</sub>Si sensor.

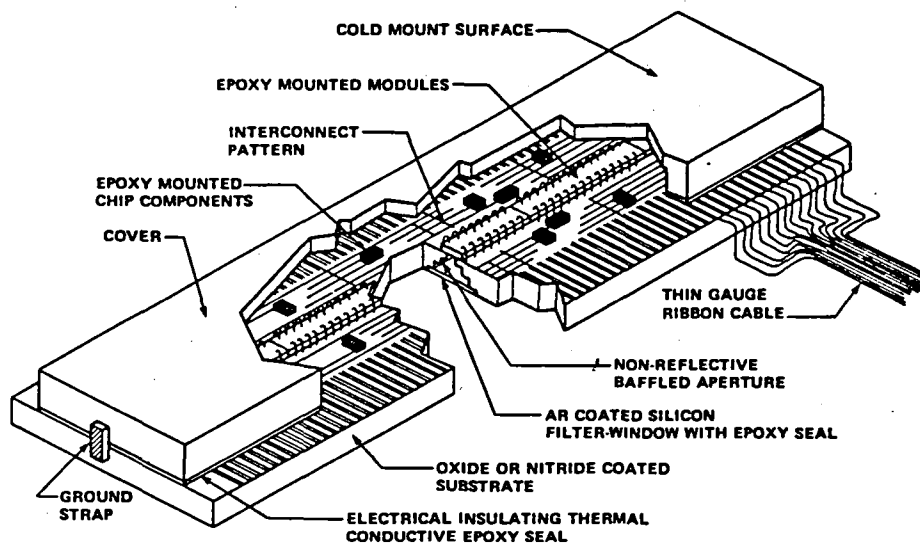


Fig. 12. MLA focal plane concept.

TABLE 4. DUAL BAND SENSOR DESIGN

Number of Detectors	2 x 512
Center-to-Center Spacing	30 $\mu$
Fill Factor	80-90%
Projected Quantum Efficiency	
$\lambda = 1.25$	20%
$\lambda = 1.65$	14%
$\lambda = 2.22$	5.5%
Operating Temperature	120K
Dark Current (120K)	2 nA/cm <sup>2</sup>
Signal-to-Noise Ratio (at 705 Km altitudo) <sup>†</sup>	200-555
Pixel Loss at Seam	2
MTF at Nyquist Frequency	65%
X, Y, Z Alignment Tolerances	< 5 $\mu$ /Chip
Power Dissipation (On-Chip)	11 mW

<sup>†</sup>Employing NASA specified nominal irradiance/integration time.

Summary

In addition to the PtSi-Schottky barrier IR-CCD which we have previously developed for thermal imaging (NEAT) applications; we have presented here our recent results on first generation Pd<sub>2</sub>Si IR-CCDs. The Pd<sub>2</sub>Si-FPA is intended for NEAT applications in the SWIR spectral range at intermediate temperatures. The Pd<sub>2</sub>Si-FPA may also be used in the NEAT application of hot target detection and discrimination in early warning satellites [14].

Table 5 demonstrates the different staring FPA technologies available. From the point of view of adequacy to space applications requiring passive cooling the Schottky barrier and HgCdTe technologies offer feasibility. Monolithic Schottky barrier arrays, however, are more suitable for high density sensors with large numbers of elements. We have demonstrated that the responsivities of Schottky barrier arrays meet the NEAT requirements for accurate classification of earth resources features. We have detailed our concept for an MLA instrument SWIR focal plane utilizing high-density dual band Pd<sub>2</sub>Si detector arrays.

TABLE 5. STARING FPA TECHNOLOGIES

	IR BAND	OPERATING TEMPERATURE	TYPE OF FPA	TYPICAL NUMBER OF ELEMENTS
(Hg, Cd) Te	3 - 5 μm 8 - 10 μm	77 (to 190) K 77K	HYBRID MONOLITHIC CID (area) CCD (line)	32 x 32 64 x 64
InSb OR InAsSb	3 - 5 μm 3 - 4 μm	77K	HYBRID MONOLITHIC CID (area) CCD (line)	32 x 32 64 x 64
EXTRINSIC In:Si  Ga:Si	3 - 5 μm 8 - 14 μm	45K 25K	HYBRID MONOLITHIC CCD	32 x 32 64 x 64
PtSi SCHOTTKY	3 - 6 μm	77K (40 - 90K)	MONOLITHIC CCD	32 x 64 64 x 128 256 x 1
Pd <sub>2</sub> Si SCHOTTKY	1 - 3.5 μm	40 - 145K	MONOLITHIC CCD	32 x 64 64 x 128

Acknowledgment

The authors wish to acknowledge the basic IR-CCD technology development supported by the Air Force Rome Air Development Center, Hanscom AFB, MA, Dr. F. Shepherd contract monitor.

The encouragement of F.B. Warren, Manager of the Systems Laboratory of the Advanced Technology Laboratories is appreciated. The assistance of the RCA Automated Systems Division, Burlington, MA, in producing the test imagery is gratefully acknowledged.

### References

1. H. Elabd, T. Villani, and W.F. Kosonocky, "Palladium-Silicide Schottky-Barrier IR-CCD For SWIR Applications at Intermediate Temperatures," IEEE ED Letters, 3, April (1982)
2. H. Elabd, "Multispectral Earth Imaging: Applications of Metal Silicide Schottky-Barrier Mosaic Sensors," presented at the AAS – 20th Goddard Memorial Symposium Meeting, March (1982).
3. D.D. Norris and J.B. Wellman, "Earth Sensing Technology" GOMAC Digest of Paper, 74 (1980).
4. R.D. Thom, T.L. Koch, J.D. Langan, and W.J. Parrish, "A Fully Monolithic InSb Infrared CCD Array," IEEE ED Trans. 27, 160 (1980).
5. K. Chow, J.D. Blackwell, J.P. Rode, D.H. Sieb, W.N. Lin, "Source-Coupling for Hybrid Focal Planes," SPIE, Vol. 282, Tech. Issues in FPA Development, 60 (1981).
6. J. Stobie, S. Iwasa, "1.0 to 2.5 micrometer Short Wavelength Infrared (SWIR) Linear Array Technology For Low Background Applications," SPIE Vol. 282, Tech. Issues in FPA Development, 98 (1981).
7. Herbert Richard, "Solid State Instrumentation Concepts for Earth Resource Observation," AAS-20th Goddard Memorial Symposium, March (1982).
8. Paul Heffner, et al., "Advanced Technology for Earth Observation Data Processing AAS," AAS-20th Goddard Memorial Symposium, March 1982).
9. Private communications with Mr. Oscar Weinstein, NASA, GSFC.
10. J.L. Engel, "Thematic Mapper – An Interim Report on Anticipated Performance," AIAA Publications, "Sens. Syst. for the 80's Conference," Colorado Springs Co., 25, December (1980).
11. B.F. Robinson, R.E. Buckley, and J.A. Burgess, "Performance Evaluation and Calibration of a Modular Multiband Radiometer for Remote Sensing Field Research," SPIE, Vol. 308, Contemporary Infrared Standards and Calibration, 146 (1981).
12. W.F. Kosonocky, H. Elabd, H. Erhardt, F. Shallcross, T. William, J. Groppe, M. Cantella, J. Klein, "Design and Performance of a 64 x 128 PtSi Schottky-Barrier IRCCD Focal Plane Array," SPIE Sym. – Infrared Sensor Technology Session, May (1982).
13. S. Goldfarb, D. Colvin, "A Large Hybrid Electro-optical Array," Int. J. For Hybrid Microelectronics, Vol. 3, 75 (1980).
14. R.D. Hudson and J.W. Hudson, "The Military Applications of Remote Sensing by Infrared," Proceedings of the IEEE, 63, 104 (1975).